IASS-IACM 2012
GF Sarajevo, Bosnia and Herzegovina
Ibrahimbegovic, Dolarevic, Hrasnica,
Madzarevic, Zlatar (eds.)

An Equilibrium Shell Element for Folded Plate Structures

E.A.W. Maunder[1], B.A. Izzuddin[2], A.C.A. Ramsay[3]

[1] *College of Engineering, Mathematics & Physical Sciences, University of Exeter, Harrison Building, North Park Road, Exeter, EX4 4QF, UK, e.a.w.maunder@exeter.ac.uk*

[2] *Department of Civil & Environmental Engineering, Imperial College London, SW7 2AZ, UK, b.izzuddin@imperial.ac.uk*

[3] *Ramsay Maunder Associates, Trehill House, Kenn, Exeter, EX6 7XJ, UK, angus_ramsay@ramsay-maunder.co.uk*

Abstract — This paper concerns the verification, validation, and performance of a hybrid equilibrium flat shell quadrilateral element for linear elastic analyses. A benchmark plate bending problem and a folded plate problem are modelled using equilibrium and conforming elements for comparison. In models of the latter problem, torsional moments are released along fold lines, and the effects of this assumption are studied by analysing a model composed of solid brick elements. A 1D hybrid equilibrium element is proposed to simplify the modelling of folded or stiffened plates.
Key-words — strong equilibrium, flat shell elements, folded plates.

1 Introduction

Equilibrium elements for modeling the membrane and bending behaviours of thin plates were formulated in the 1960's and 70's by, for example, Fraeijs de Veubeke et al [1-3]. Potential problems due to spurious kinematic modes were avoided generally by using the concept of macro-elements, for example quadrilateral elements were formed by assembling four triangular elements with sides aligned with the diagonals of the quadrilateral, although this was realized to be unnecessary in the case of plate bending governed by Kirchhoff theory. In the 1990's Almeida and Freitas [4] proposed a general hybrid formulation for equilibrium elements. The inherent stability of quadrilateral plate macro-elements was recognized by Maunder et al [5] in the context of this type of hybrid formulation. Equilibrium models have been used in error analysis, by exploiting dual analyses, and in design, by appealing to the lower bound theory of plasticity: moreover, they may offer numerical benefits, such as freedom from locking etc..

However, to the authors' knowledge, these types of element have not been combined into flat shell elements in order to model folded plates. In this paper, the term folded plate will be used to mean that complete continuity exists in the 3D continuum sense where non-coplanar plates are connected. However, thin plates governed by Reissner-Mindlin theory will be assumed with flat shell elements without recourse to using drilling freedoms [6] or couple-stresses [7]. The hybrid equilibrium flat shell element has 6 rigid body kinematic freedoms for each side, but torsional moments cannot be codiffusive along a fold without invoking couple-stresses. A simpler way to model such connections, and maintain codiffusive tractions, is to release the torsional moments along a fold.

This paper is only concerned with linear elastic behaviour. It should be noted that although the computations have been carried out using the non-linear software ADAPTIC developed by the second author [8], loads have been specified at a low value so that non-linear effects can be neglected. The outline of the paper is as follows. It continues in Section 2 with a summary of a formulation of hybrid equilibrium elements. Section 3 provides evidence to verify the formulation, and to indicate performance characteristics in a plate bending benchmark problem. In Section 4 a folded plate problem is considered and results are compared with those from conforming models based on plate elements or solid hexahedral elements. Proposals are presented in Section 5 for a general 1D hybrid equilibrium element to provide a simpler way to

model the complete interactions between non-coplanar equilibrium flat shell elements. Section 6 forms the closure of the paper.

2 Formulation of a hybrid equilibrium quadrilateral element

The aim of a hybrid equilibrium finite element model is to produce a strong form of equilibrium by connecting statically admissible internal fields of stress-resultants within elements in a codiffusive way. Following [4], this is achieved by the use of boundary displacement fields defined independently for each side of an element, resulting in potentially non-codiffusive tractions being zeroed as a consequence of doing zero work with the side displacements.

Stress and displacement fields are represented in Equation (1).

$$\boldsymbol{\sigma} = \boldsymbol{S} \cdot \boldsymbol{s} + \boldsymbol{\sigma}_p, \text{ and } \boldsymbol{\delta} = \boldsymbol{V} \cdot \boldsymbol{v} \tag{1}$$

$\boldsymbol{S}$ and $\boldsymbol{V}$ represent bases for stress-resultants and boundary displacements with parameters $\boldsymbol{s}$ and $\boldsymbol{v}$ respectively. $\boldsymbol{\sigma}_p$ represents a particular field of stress-resultants which equilibrates with load distributed over the surface of an element. The parameters $\boldsymbol{v}$ represent modes of side displacement for all sides of an element, and the modes are based on complete Legendre polynomials up to a degree which is the same as the degree of the corresponding stress-resultants.

Dual modes of side traction correspond to resultant forces and/or moments and self-balancing modes of traction. The distributions of traction which equilibrate with $\boldsymbol{S.s}$ are denoted by $\boldsymbol{t}$, and these are related to the stress parameters and traction modes $\boldsymbol{g}$ as in Equation (2).

$$\boldsymbol{t} = \bar{\boldsymbol{S}} \cdot \boldsymbol{s} \text{ and } \boldsymbol{g} = \oint_{\boldsymbol{\Gamma}} \boldsymbol{V}^{\boldsymbol{T}} \cdot \boldsymbol{t} \cdot \boldsymbol{d\Gamma} \tag{2}$$

Weak compatibility conditions between internal strains and side displacements are expressed by Equations (3).

$$\int_{\boldsymbol{\Omega}} \boldsymbol{S}^{\boldsymbol{T}} \cdot \boldsymbol{\varepsilon} \cdot \boldsymbol{d\Omega} = \oint_{\boldsymbol{\Gamma}} \bar{\boldsymbol{S}}^{\boldsymbol{T}} \cdot \boldsymbol{\delta} \cdot \boldsymbol{d\Gamma} \quad \text{or} \quad \boldsymbol{F} \cdot \boldsymbol{s} + \boldsymbol{e}_p = \boldsymbol{D}^{\boldsymbol{T}} \cdot \boldsymbol{v} \tag{3}$$

where $\boldsymbol{F} = \int_{\boldsymbol{\Omega}} \boldsymbol{S}^{\boldsymbol{T}} \cdot \boldsymbol{C} \cdot \boldsymbol{S} \cdot \boldsymbol{d\Omega}$, $\boldsymbol{e}_p = \int_{\boldsymbol{\Omega}} \boldsymbol{S}^{\boldsymbol{T}} \cdot \boldsymbol{C} \cdot \sigma_p \cdot \boldsymbol{d\Omega}$, and $\boldsymbol{D}^{\boldsymbol{T}} = \oint_{\boldsymbol{\Gamma}} \bar{\boldsymbol{S}}^{\boldsymbol{T}} \cdot \boldsymbol{V} \cdot \boldsymbol{d\Gamma}$, and $\boldsymbol{C}$ denotes the compliance matrix in $\boldsymbol{\varepsilon} = \boldsymbol{C} \cdot \boldsymbol{\sigma}$.

If applied tractions $\bar{\boldsymbol{t}}$ and tractions $\boldsymbol{t}_p$, which equilibrate with the particular stress-field $\boldsymbol{\sigma}_p$, are polynomials of degree less than or equal to the degree of the side displacements, then strong equilibrium between side tractions and internal stress fields is enforced by:

$$\oint_{\boldsymbol{\Gamma}} \boldsymbol{V}^{\boldsymbol{T}} \cdot \bar{\boldsymbol{t}} \cdot \boldsymbol{d\Gamma} - \oint_{\boldsymbol{\Gamma}} \boldsymbol{V}^{\boldsymbol{T}} \cdot \boldsymbol{t}_p \cdot \boldsymbol{d\Gamma} = \boldsymbol{g} = \boldsymbol{D} \cdot \boldsymbol{s} \tag{4}$$

The stiffness matrix $\boldsymbol{K}$ of an element is formed by elimination of $\boldsymbol{s}$ from Equations (3) and (4), so that:

$$\boldsymbol{K} \cdot \boldsymbol{v} = \boldsymbol{g} + \boldsymbol{D} \cdot \boldsymbol{F}^{-1} \boldsymbol{e}_p \text{ where } \boldsymbol{K} = \boldsymbol{D} \cdot \boldsymbol{F}^{-1} \cdot \boldsymbol{D}^{\boldsymbol{T}} \tag{5}$$

The results reported in this paper are due to quadrilateral elements with internal stress-resultants composed of piecewise linear fields of membrane forces and transverse shear forces, together with piecewise quadratic moment fields. Displacement fields are described with reference to the displacements (u,v,w) along the directrix, and the rotations (ϕ_n,ϕ_s) of the rulings on the rectangular surface formed by a side of an element. These are illustrated in Figure 1.

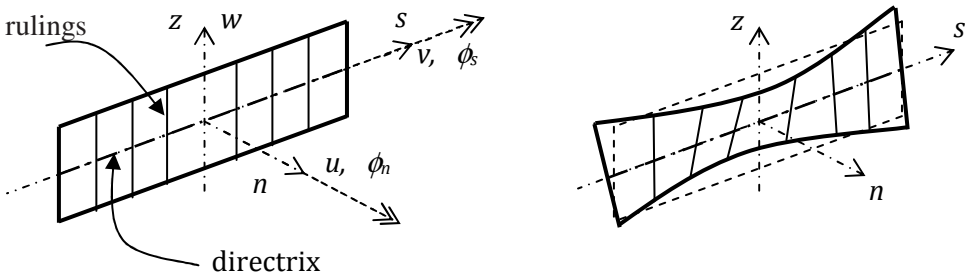

FIG. 1: Surface displacements and deformations of a side.

Codiffusive tractions are ensured by using complete linear displacement and quadratic rotation fields. Thus there are defined 6 rigid body modes plus 6 deformational modes comprising one uniform tensile strain ε_s, rotations ϕ_s of degrees 1 and 2, rotations ϕ_n of degrees 0, 1, and 2. The total number of kinematic degrees of freedom is then given by $n_v = 4\times12 = 48$. The number of independent fields of stress-resultants is given by $n_s = 7 + 17 = 24$ [9], and thus there would exist $(24 - 6) = 18$ spurious kinematic modes. As originally proposed by the Liege school [2,3], such modes can be effectively blocked by combining 4 triangular hybrid elements into a quadrilateral. For the displacements under consideration, this combination must be based on the internal sides being aligned to form the diagonals of the quadrilateral. As noted [5,10], this condition on alignments is not required for higher degree quadrilateral elements. Internal freedoms are condensed out, leading to a 48×48 element stiffness matrix, and further details can be seen in Maunder & Izzuddin [11].

3 Performance in a benchmark problem

A benchmark problem for plate bending behaviour is selected and comparisons made with theoretical solutions or solutions from conforming finite elements. A square soft simply supported plate is considered with 8m side length, 0.25m thickness, E = 2.1e8 kN/m^2 , and ν = 0.3. A uniformly distributed load of 1e-6 kN/m^2 is applied to the plate, and one quadrant is modelled with a sequence of uniform meshes. The initial mesh consists of a single element, this is then refined to a 64×64 mesh. This problem leads to local large gradients of stress resultants, but there are no singularities [12]. Figures 2a and 2b contain contour plots from the finest mesh. These are similar to those from a conforming model using the same mesh of 9-noded Lagrange elements, and so this is taken as a reference solution.

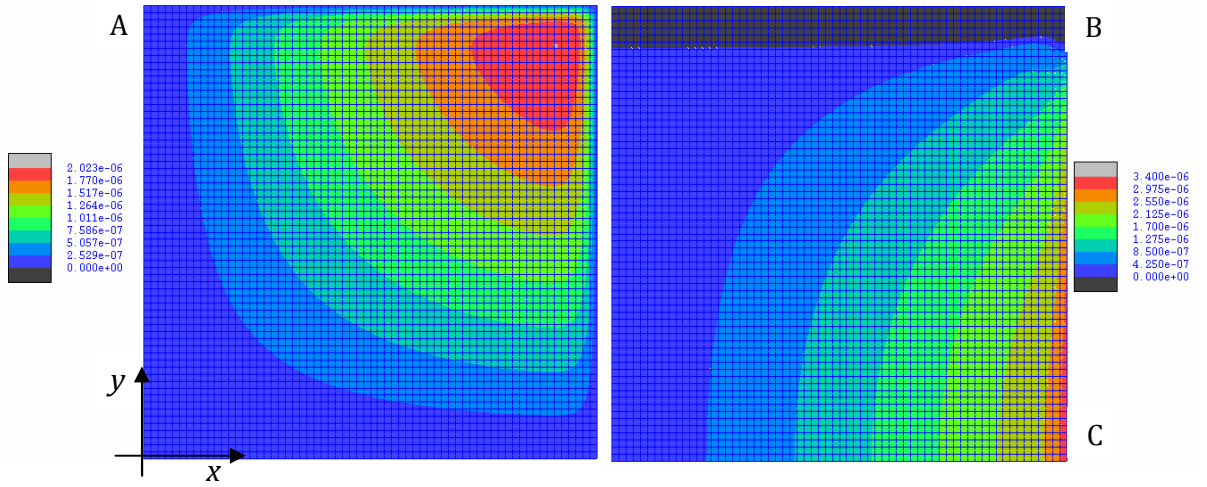

Mxy kNm/m contours *Qxz* kN/m positive contours

FIG. 2a: "reference" solution from 64x64 uniform mesh of hybrid equilibrium plate elements of moment degree 2, or 9-noded conforming elements of degree 2.

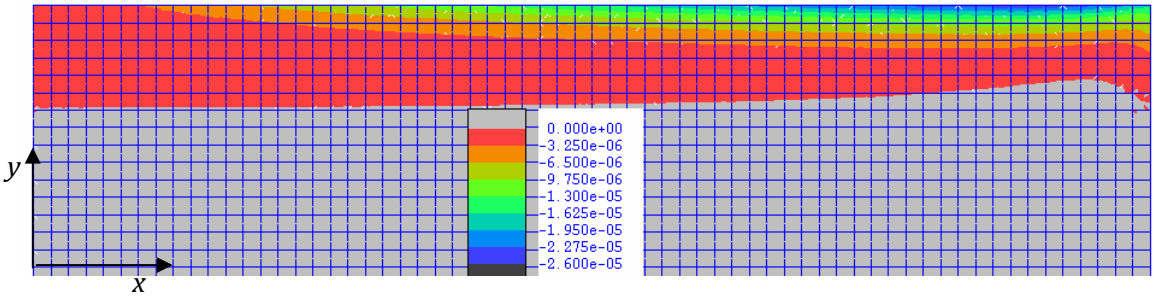

FIG. 2b: *Qxz* negative contours in a boundary layer where the shear force is concentrated.

The convergence of strain energy and the extreme values of transverse shear stress resultants are compared for the equilibrium and conforming models in Figure 3.

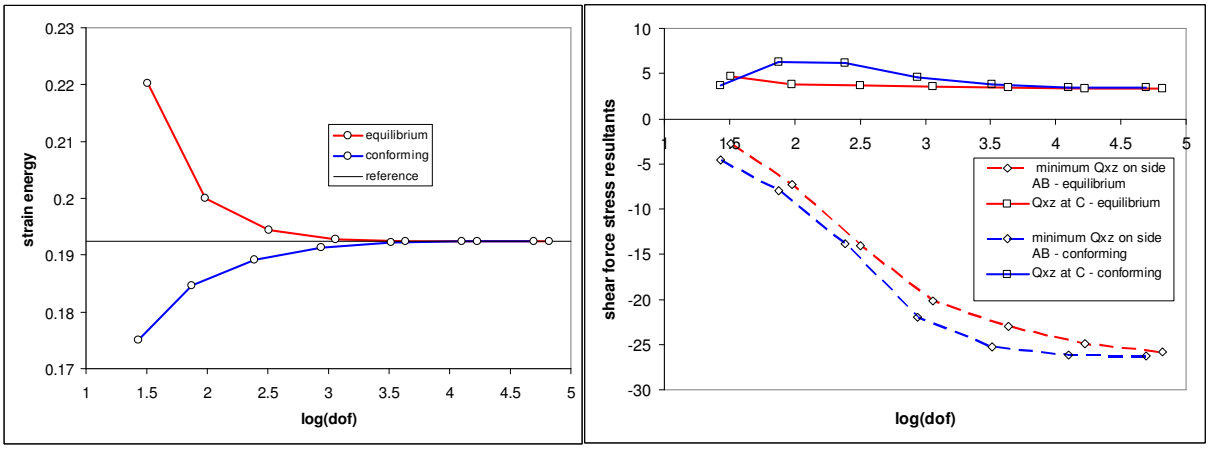

FIG. 3: Convergence of (i) strain energy kNm ($\times 10^{15}$) for a quadrant, (ii) shear force kN/m ($\times 10^{6}$) - minimum shear *Qxz* on side AB, and shear *Qxz* at C.

It is noted that, for these quadratic elements, convergence may be considered to have occurred, for practical purposes, when the element size is equal to its thickness. The corresponding mesh is 16x16, and the numbers of dof are then 4352 (log 4352 = 3.639) and 3267 (log 3267 = 3.514) for the equilibrium and conforming models respectively. The relative difference in energies for the finest mesh is 1 part in 10^5. It may be concluded that the quadratic equilibrium element provides solutions of comparable quality to that from the 9-noded Lagrange conforming element for this benchmark problem. However, the strain energies provide, as expected, upper and lower bounds to the exact strain energy. Hence complementary use of both models should provide an effective error estimator.

4 Study of a folded plate problem

A folded plate is shown in Figure 4, where each plate is 4m square with thickness 0.25m, E = 2.1e8 kN/m^2, and ν = 0.3. The fold angle along BE is 90º. Soft simple supports are assumed along sides AB and BC, and a uniform line load W = 40e-6 kN/m is applied in the direction of BA along the 0.5m length of side adjacent to F. Each of the plates is initially modelled by a uniform mesh of 8×8 square flat shell elements that combine both membrane and plate bending fields.

Along a fold where two non-planar elements are connected, all tractions can be made codiffusive with the exception of the torsional moments. In order to ensure that a model is completely in equilibrium in terms of stress-resultants, the torsional moments are released along a fold. From the kinematic point of view, the corresponding drilling rotations of the normals are unconstrained, at least where 2 plates are involved. For connections between 3 or more plates, the rotations would be coupled with 2 degrees of freedom.

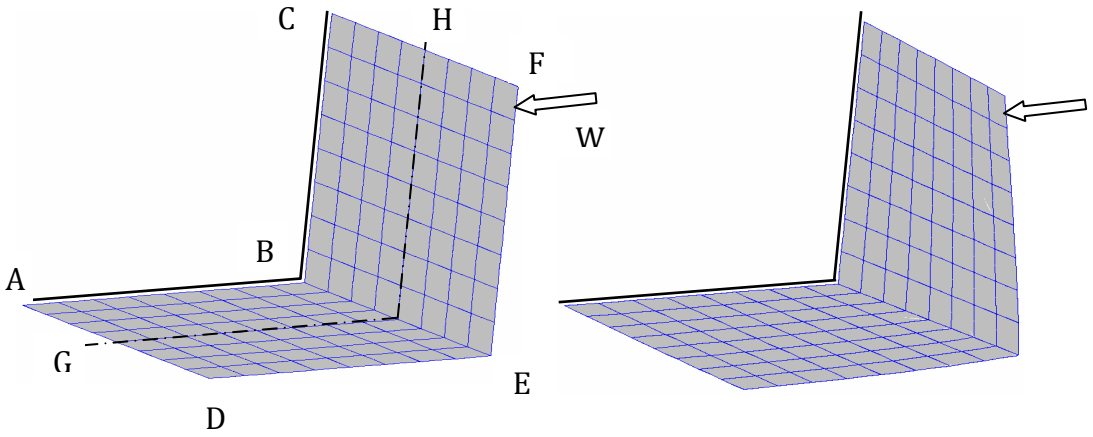

FIG. 4: Initial mesh of the folded plate and its deformed shape

A physical model can be defined using a biological analogy with a spinal column articulated with a central cord connecting a set of vertebrae (segments) which can allow independent degrees of movement. This is illustrated in Figure 5.

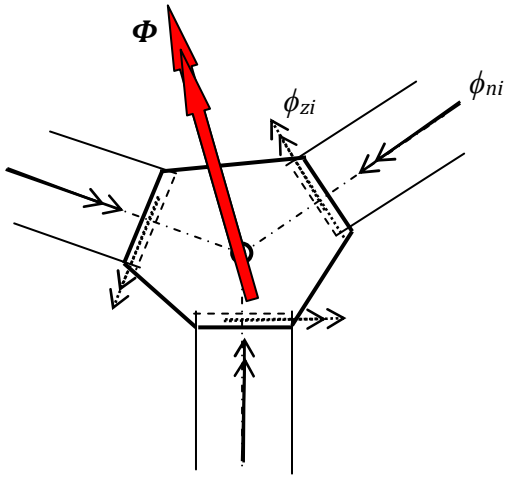

FIG 5: Articulation to free the transference of drilling components of rotation ϕ_z.

The rotation $\boldsymbol{\Phi}$ of the segment is resolved into components ϕ_{ni} and ϕ_{zi} to correspond to the rotations of the rulings in side *i* so that the component ϕ_{ni} is transferred, but the component ϕ_{zi} is not transferred – the ruling is attached to the vertebra by a cylindrical type of bearing which allows free rotation of ϕ_{zi} within the vertebra.

In this way the rotations ϕ_{ni} are not generally independent, but are dependent on the 2 degrees of freedom associated with the rotation vector $\boldsymbol{\Phi}$ of a vertebra. Note that if only two elements are connected along a spine, then rotation components ϕ_{n1} and ϕ_{n2} are generally independent and free unless the elements are coplanar. In that case $\phi_{n1} = \phi_{n2} = \boldsymbol{\Phi}$.

The conforming flat shell element generally has 3 translational dof per node but only 2 rotational dof when the drilling freedom is ignored. Only nodes common to non-planar elements account for 3 rotational dof since rotations about an axis normal to the fold axis can be resisted by moments in at least one of the elements. However, rotational equilibrium of nodes on the fold axis requires zero nodal moments to be transferred about an axis normal to the fold from either of the two plates. Thus in a discrete sense, nodal torsional moments are released, and in the limit as a mesh is refined, the distributions of torsional moments along the fold axis tend to zero. The two models using the equilibrium and conforming models again tend to the same solution as the mesh is refined, and this is illustrated for strain energy in Figure 6. The relative difference in energies for the finest mesh is 1 part in 3,000.

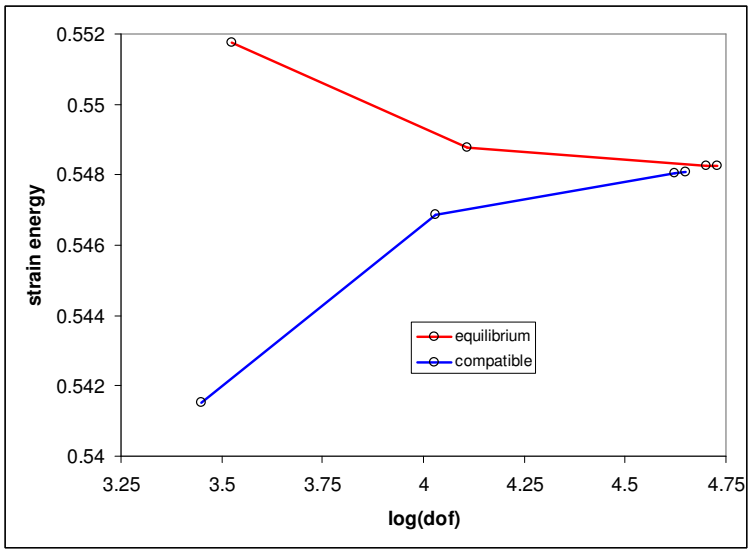

FIG. 6: Convergence of strain energies – kNm ($\times 10^{14}$)

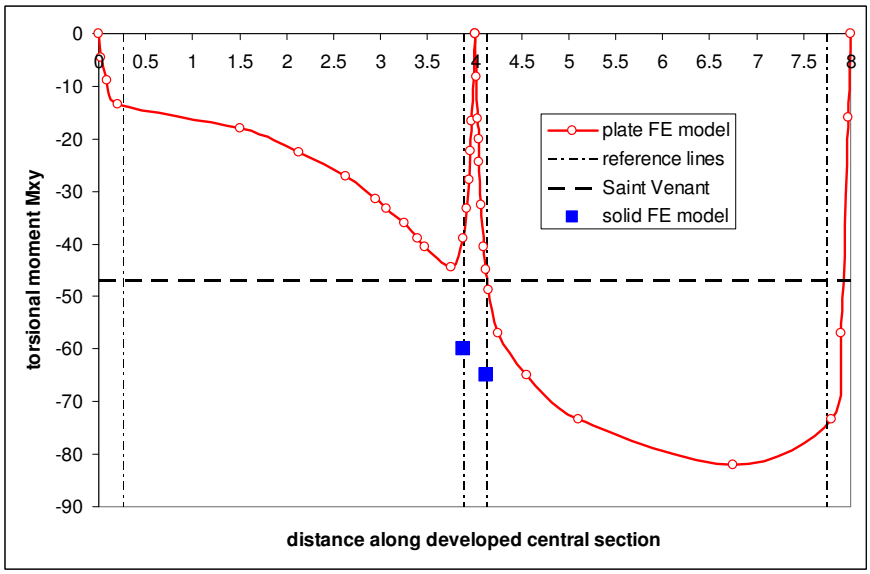

FIG. 7: *Mxy* kNm/m ($\times 10^{7}$) at centre cross-section GH in FIG. 4

The two points in Figure 7 denoted by ■ represent values of torsional moment derived from the solid FE model at the intersections of the plates with the spine zone. The dashed line in Figure 7 represents the uniform intensity of torsional moment corresponding to the use of Saint Venant theory for torsion of a thin walled section assuming unrestrained warping. The reference lines correspond to distances from the ends of the section equal to 0.25m, i.e. the thickness of the plate. The reference lines adjacent to the fold line correspond to the interfaces of the plates with the spine.

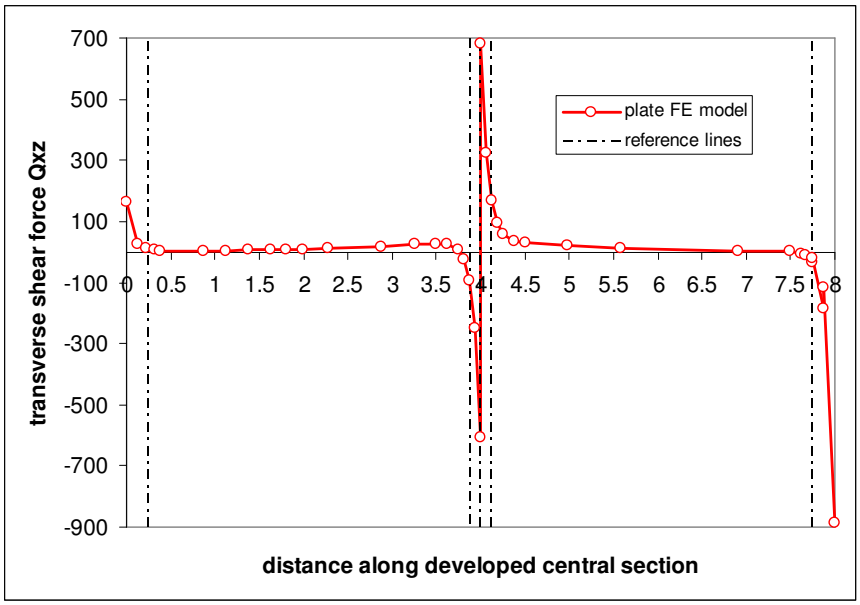

FIG. 8: *Qxz* kN/m (×10⁷) at centre cross-section GH in FIG. 4

As shown in Figures 7 to 9, the solutions for Mxy and Qxz adjacent to the fold line indicate boundary layers similar to those obtained adjacent to soft simple supports. These quantities have high local gradients within a width of plate generally less than the plate thickness, or approximately within the intersection subdomain of the two plates when considered as a solid in 3D space.

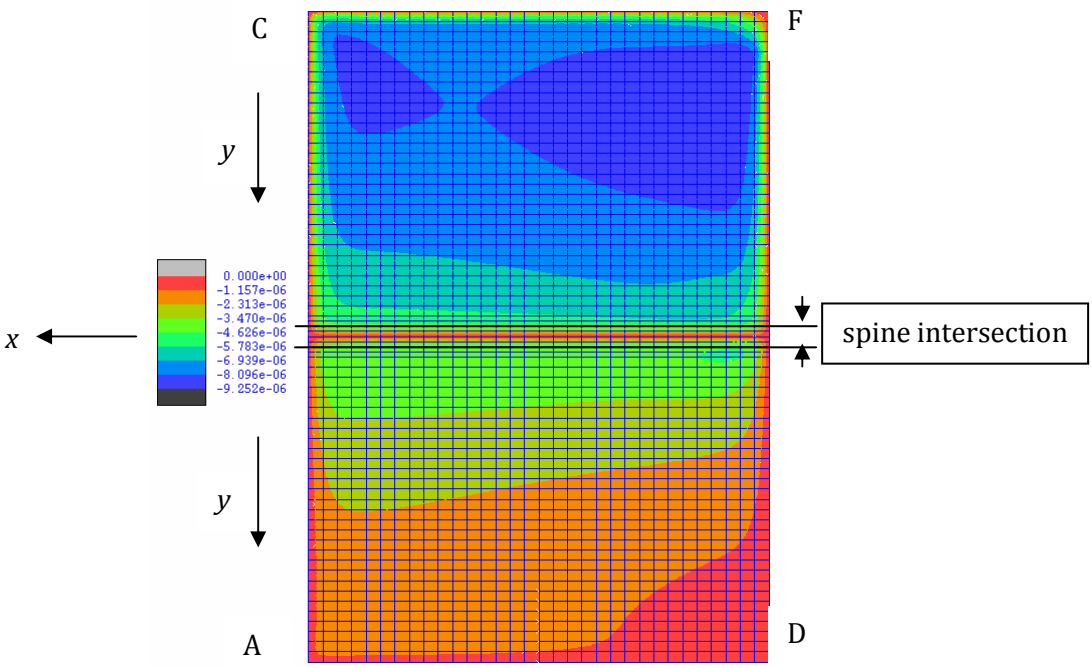

FIG. 9: contour plot of *Mxy* kNm/m, view towards fold at 45º to planes of each plate.

In order to understand the transmission of torsional moments through this subdomain, a solid model composed of 20 node conforming hexahedral elements was analysed. This model was based on the use of two elements through the thickness, i.e. the height of all elements was taken as 0.125m. The mesh was uniform with square elements in plan of dimension 0.25m except around the perimeters where one dimension was reduced in two stages to 0.0625m in order to improve modelling of the behaviour within the boundary layers.

Although this model has only 1680 hexahedral elements, and is not therefore expected to produce accurate stresses, the model is constructed with three subdomains, one each to represent a plate, and one to represent the spine or intersection zone. These subdomains are shown in Figure 10, and they are coupled at the 165 nodes at each interface so that the corresponding nodal forces that satisfy the weak equilibrium conditions are output. These forces can then be used to recover equilibrating stress-resultants acting on and within the spine.

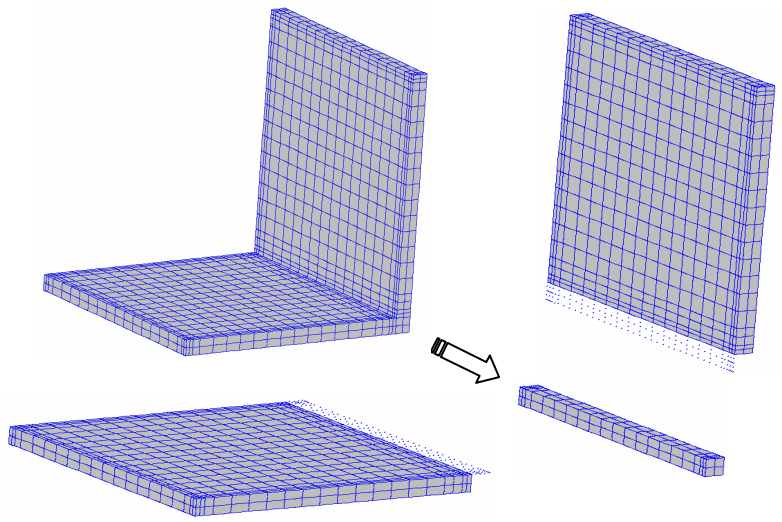

FIG. 10: Exploded view of the solid finite element model.

Comparisons are now made in Figure 11 between the torsional moments transmitted to the spine from the horizontal plate, and the total vertical tractions acting on the spine, as given by the plate and solid models.

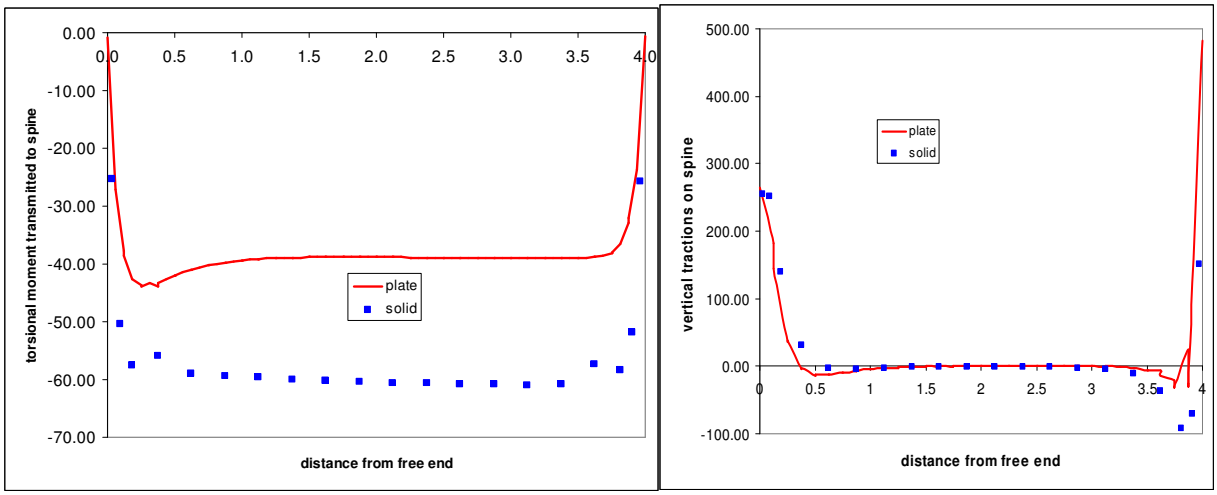

FIG. 11: results for *Mxy* kNm/m ($\times 10^7$) from horizontal plate,
and vertical tractions on spine kN/m ($\times 10^7$) .

Although the values of the torsional moments are different, their distributions are very similar in that this moment is almost constant along the spine except adjacent to the ends. This implies that these moments are transferred along the spine to its ends with a consequent constant vertical shear force within the spine, which is confirmed by the shear force diagram in Figure 12.

In terms of stress-resultants acting on and within the spine, the plate and solid models thus indicate the same mechanism for the transfer of torsional moments, with the plate model probably influenced by a reduced effective spine stiffness due to the assumed release of torsion at the centre of the spine.

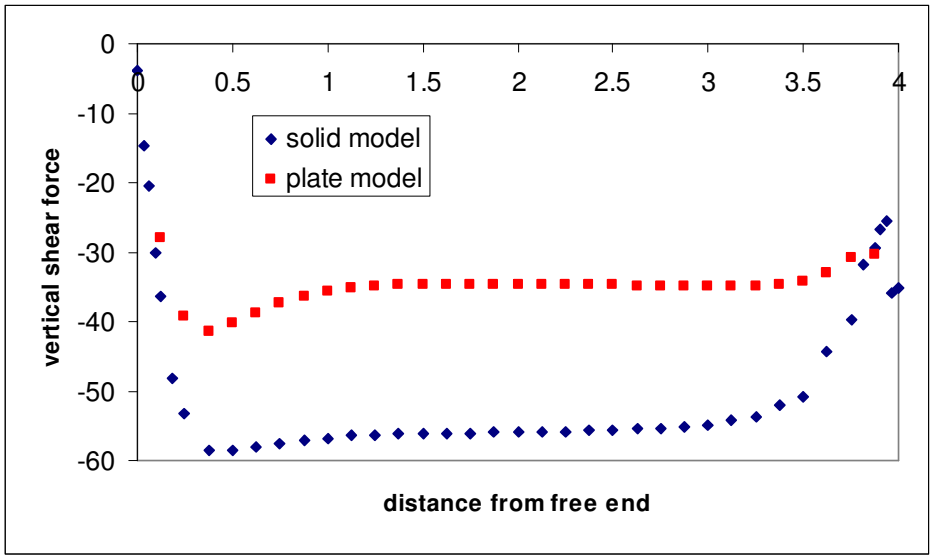

FIG. 12: Vertical shear force kN ($\times 10^7$) diagram for the spine.

5 Proposals for a general spine element

The spine as described in the previous sections has been used as a device to explain the kinematic connections between hybrid plate elements when torsional moments are released at the fold line. However, the concept of a spine element can be developed as a 1D hybrid equilibrium element with the ability to accept non-zero torsional moments and transfer internal stress resultants along its length. As regards the physical analogy, the vertebrae become connected and interact with each other.

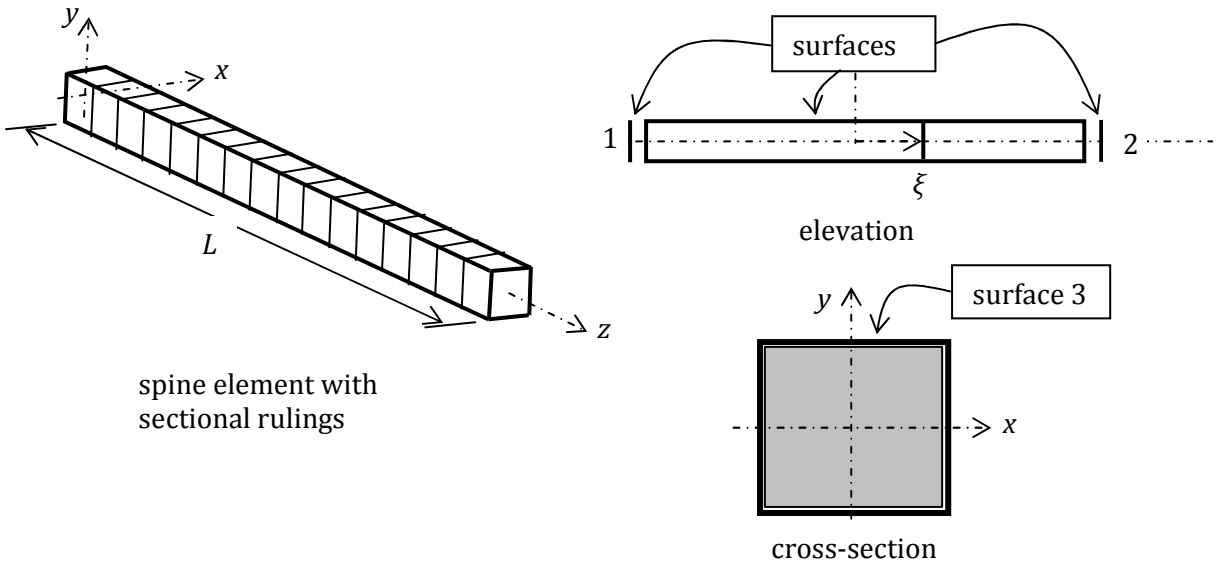

FIG. 13: spine element

The 1D element is a development from earlier ideas proposed by Robinson for a mode-amplitude technique [13,14], but recast in the mould of a hybrid equilibrium element with independent kinematic variables. With reference to Figure 13, consider a prismatic element with an axis, or directrix, and a surface formed by a generatrix, a closed perimeter curve that takes the place of the rulings on the side of a plate element. The total closed surface is made up of three parts, two end sections numbered 1 and 2 that are assumed to remain rigid each having 6 kinematic degrees of freedom, and the surface numbered 3 formed by the generatrix. Each

perimeter ruling can have up to 6 kinematic displacements (3 translations and 3 rotations) that are functions of a parameter ξ which represents the position of a ruling along the directrix. The side displacements of adjacent plate elements must be identified with those of the spine surface along its length, the end displacements of a spine element are identified with adjacent spine elements.

The kinematic relations in Equation (1) now take the form in Equation (6) for an element with rotation functions of degree p:

$$\boldsymbol{\delta} = \begin{Bmatrix} \boldsymbol{\delta}_1 \\ \boldsymbol{\delta}_2 \\ \boldsymbol{\delta}_3(\boldsymbol{\xi}) \end{Bmatrix} = \boldsymbol{V} \cdot \boldsymbol{v} \quad \text{where} \quad \boldsymbol{V} = \begin{bmatrix} \boldsymbol{V_1} \\ \hline \boldsymbol{V_2} \\ \hline \boldsymbol{V_3} \end{bmatrix} \tag{6}$$

and $\boldsymbol{V}_1 = \begin{bmatrix} \boldsymbol{I_6} \mid \boldsymbol{0} \mid \boldsymbol{0} \end{bmatrix}$, $\boldsymbol{V}_2 = \begin{bmatrix} \boldsymbol{0} \mid \boldsymbol{I_6} \mid \boldsymbol{0} \end{bmatrix}$, $\boldsymbol{V_3} = \left[\begin{array}{cccc|ccc|ccc} 0 & 0 & 0 & 0 & P_0 & \cdots & P_{p-1} & 0 & \cdots & 0 & 0 \\ 0 & 0 & 0 & 0 & 0 & \cdots & 0 & P_0 & \cdots & P_{p-1} & P_p \end{array}\right] \otimes \boldsymbol{I}_3$.

$\boldsymbol{\delta}_1$ and $\boldsymbol{\delta}_2$ denote the displacement vectors of ends 1 and 2, and $\boldsymbol{\delta}_3(\xi)$ denotes the displacement vector of the perimeter ruling at position ξ between the ends. In general, $\boldsymbol{\delta}$ has dimension 9, and the displacement vectors are arranged with 3 translational components followed by 3 rotational components. P_j denotes the Legendre interpolation polynomial of degree j, and $\boldsymbol{I}_n$ denotes the $n \times n$ unit matrix in the Kronecker product. The dimension of the displacement parameter vector $\boldsymbol{v}$ is $n_v = (6 + 6 + 3p + 3(p + 1)) = 15 + 6p$.

The internal stress fields are described in terms of up to 6 stress-resultants, i.e. an axial force, two transverse shear forces, a torsional moment, and two bending moments. The static relations in Equation (1) now take the form in Equation (7).

$$\boldsymbol{\Sigma} = \begin{Bmatrix} \Sigma_x \\ \Sigma_y \\ \Sigma_z \\ \hline M_x \\ M_y \\ M_z \end{Bmatrix} = \boldsymbol{S}.\boldsymbol{s} \text{ where } \boldsymbol{S} = \left[\begin{array}{ccc|ccccc} P_0 & \cdots & P_p & 0 & \cdots & 0 & 0 \\ \hline 0 & \cdots & 0 & P_0 & \cdots & P_p & P_{p+1} \end{array}\right] \otimes \boldsymbol{I}_3, \tag{7}$$

and the degree of the stress parameter vector $\boldsymbol{s}$ is $n_s = (3(p + 1) + 3(p + 2)) = 9 + 6p$.

The degrees of the force and moment fields are one higher than the corresponding form of displacement to enable equilibrium to be satisfied between internal actions and external actions dual or conjugate to the displacements of the surface of the spine. The differential equilibrium conditions take the form of Equation (8).

$$\left[\begin{array}{ccc|ccc} d/dz & 0 & 0 & 0 & 0 & 0 \\ 0 & d/dz & 0 & 0 & 0 & 0 \\ 0 & 0 & d/dz & 0 & 0 & 0 \\ \hline 0 & -1 & 0 & d/dz & 0 & 0 \\ 1 & 0 & 0 & 0 & d/dz & 0 \\ 0 & 0 & 0 & 0 & 0 & d/dz \end{array}\right] \begin{Bmatrix} \Sigma_x \\ \Sigma_y \\ \Sigma_z \\ \hline M_x \\ M_y \\ M_z \end{Bmatrix} + \begin{Bmatrix} N_x \\ N_y \\ N_z \\ \hline C_x \\ C_y \\ C_z \end{Bmatrix} = \begin{Bmatrix} 0 \\ 0 \\ 0 \\ \hline 0 \\ 0 \\ 0 \end{Bmatrix}, \text{ or } \boldsymbol{\Delta}.\boldsymbol{\Sigma} + \boldsymbol{N} = \boldsymbol{0} \tag{8}$$

where N_x, N_y, N_z, denote force components per unit length, and C_x, C_y, C_z denote couple components per unit length, applied to surface 3. Of course Equation (8) is still a weak form of equilibrium in that it involves stress-resultants rather than stress tensors. However, it provides

a flexible connection between plates, whether coplanar or not, and could also represent a stiffening spar or beam component.

The compatibility Equation (3) now contains $\boldsymbol{D^T}$ as defined in Equation (9):

$$\boldsymbol{D^T} = \left[-\boldsymbol{S^T}(0)\cdot\boldsymbol{V}_1 + \boldsymbol{S^T}(1)\cdot\boldsymbol{V}_2 - \int_0^{\boldsymbol{L}} [\boldsymbol{\Delta}\cdot\boldsymbol{S}(\boldsymbol{\xi})]^T \cdot \boldsymbol{V}_3(\boldsymbol{\xi})\cdot \boldsymbol{dz} \right], \tag{9}$$

the natural flexibility matrix $\boldsymbol{F}$ and element stiffness matrix $\boldsymbol{K}$ are then formed in a similar way to that defined in Equations (3) and (5).

6 Closure

- The formulation of the quadrilateral hybrid macro-equilibrium plate element based on quadratic fields of moment and linear fields of membrane and shear forces has been verified as regards modelling both bending and flat shell behaviour. Its performance appears to be comparable to that of the 9-noded conforming Lagrange element, and their complementary use should be effective in error analysis.

- Both types of element converge to the same solution for a folded plate problem when torsional moments are released along a fold line. The release of these moments leads to boundary layers adjacent to the fold line similar to those observed along soft simple supports.

- Modelling the folded plate with hexahedral elements confirms that the plate models capture the essential modes of interaction between the plates and their intersection subdomain, or spine. However, the numerical values of the tractions as stress-resultants are not yet in agreement. Further refinement of the solid model is required to study the convergence of these tractions.

- Further research is intended to verify and evaluate the performance of 1D hybrid equilibrium elements in modelling the spinal intersection subdomain.

- Further research is also planned to evaluate the use of the hybrid flat shell element in the case of geometric non-linear behaviour.

Acknowledgements

All the numerical results presented in this paper have been derived from the ADAPTIC finite element program developed by the second author at Imperial College London.

References

[1] B.Fraeijs de Veubeke, G. Sander. *An equilibrium model for plate bending*, Int. J. Solids & Structures, 4, 447-468, 1968.
[2] G. Sander. *Application of the dual analysis principle*, High Speed Computing of Elastic Structures, Volume 61, Ed. B. Fraeijs de Veubeke, 167-207, Universite de Liege, 1971.
[3] B. Fraeijs de Veubeke, G. Sander, P. Beckers. *Dual analysis by finite elements: linear and non linear applications*, Technical Report AFFDL-TR-72-93, Wright-Patterson Air Force Base, Ohio, USA, December 1972.
[4] J.P. Moitinho de Almeida, J.A. Teixeira de Freitas, *Alternative approach to the formulation of hybrid equilibrium finite elements*, Computers & Structures, 40, 1043-1047, 1991.
[5] E.A.W. Maunder, J.P. Almeida, A.C.A. Ramsay, A General Formulation of Equilibrium Macro-elements with Control of Spurious Kinematic Modes: The Exorcism of an Old Curse. Int. J. Numer. Meth. Engng., 39, 3175-3194, 1996.

[6] H. Nguyen-Van, N. Mai-Duy, T. Tran-Cong, *An improved quadrilateral flat element with drilling degrees of freedom for shell structural analysis*. Computer Modeling in Engineering & Sciences, 49, 81-112, 2009.
[7] A.C. Eringen, *Microcontinuum Field Theories I: Foundations and Solids*, Springer, 1999.
[8] B.A. Izzuddin, *Nonlinear Dynamic Analysis of Framed Structures*, PhD Thesis, Imperial College, University of London, 1991.
[9] E.A.W. Maunder, J.P. Almeida, *A triangular hybrid equilibrium plate element of general degree*, Int. J. Numer. Meth. Engng., 63, 315-350, 2005.
[10] E.A.W. Maunder, J.P. Almeida, *The stability of stars of triangular equilibrium plate elements*. Int. J. Numer. Meth. Engng., 77, 922-968, 2009.
[11] E.A.W.Maunder, B.A. Izzuddin, *Large displacement analysis of plates using hybrid equilibrium elements.* In CD Proceedings III European Conference on Computational Mechanics: Solids, Structures and Coupled Problems in Engineering, C.A. Mota Soares et.al. (eds.), Lisbon, 2006.
[12] A. Rossle, A.-M. Sandig, *Corner singularities and regularity results for the Reissner/Mindlin plate model*, Sonderforschungsbereich 404, University of Stuttgart, 2001.
[13] J. Robinson, *The mode-amplitude technique and hierarchical stress elements – A simplified and natural approach*, Int. J. Numer. Meth. Engng., 21, 487-507, 1985.
[14] J. Robinson, *Towards automated stress analysis: Finite element mode-amplitude technique,* Finite Elements in Analysis and Design, **22**, 195-210, 1996.